COMMUNICATION

Check for updates

Effect of the number ratio and size ratio on the formation of binary superlattices assembled from polymer-tethered spherical nanoparticles of two sizes†

Jinlan Li,[a,b] Xin Yu,[a,b] Jianing Zhang,[a,c] Jing Jin,*[a,c] Yanxiong Pan, [ID] *[a,b] Xiangling Ji [ID] [a,b] and Wei Jiang [ID] *[a,b,c]

Binary superlattices (BNSLs) with unique configurations are of great interest, attributed to the interaction between two kinds of nanoparticles, providing potential applications in sensing, electronic and optical fields. Here, polystyrene (PS) tethered spherical gold nanoparticles (AuNPs) with two core diameters spontaneously assembled into BNSLs via emulsion-confined self-assembly. BNSLs with specific stoichiometry and interparticle gaps of the NPs are prepared by tuning the number and size ratios of the two types of NPs. Moreover, after introducing long ligands, binary NPs are separated into macrophase separation or mixed together, depending on the interaction between polymer chains tethered to the AuNPs. Finally, PS-tethered AuNPs provide more possibilities for fabricating multifunctional BNSLs.

Introduction

Recently, the assembly of two kinds of metal nanoparticles (NPs) into well-defined binary superlattices (BNSLs) has resulted in diverse stoichiometries and lattice symmetries, leading to new properties owing to the interactions of the two kinds of nanoparticles.[1–13] Long-ordered arrays or superlattices assembled from two kinds of NPs have attracted widespread attention owing to their potential applications in sensing, photonics, and plasmonics, among others.[14–24] However, the macroscopic properties of BNSLs depend on their internal structures, which can be tuned by the structural parameters of the NPs, such as the size ratios, intrinsic shape, number ratios and the constituents of the two types of NPs.[25–34]

aState Key Laboratory of Polymer Physics and Chemistry, Changchun Institute of Applied Chemistry, Chinese Academy of Sciences, Changchun 130022, China. E-mail: jjin@wtu.edu.cn, yxpan@ciac.ac.cn, weijiang@wtu.edu.cn
bSchool of Applied Chemistry and Engineering, University of Science and Technology of China, Hefei 230026, China
cSchool of Materials Science and Engineering, Wuhan Textile University, Wuhan 430200, China
†Electronic supplementary information (ESI) available. See DOI: https://doi.org/10.1039/d4nr04032e

When designing BNSLs with unique internal structures, the physical and chemical properties of ligands decorating the surfaces of the NPs play a dominant role.[35–41] Up to now, various molecules (*e.g.*, short-chain molecules and polymers) have been used as ligands to prepare BNSLs with unique internal structures. For instance, Murray *et al.* proved that the strength of near-field couplings between oleic acid-coated NPs could be adjusted by varying the spherical nanoparticle size, composition, and internal structures of BNSLs, leading to broadband spectral tunability of the collective plasmonic response of BNSLs across the entire visible spectrum.[42] Interestingly, various soft materials are prepared when polymers are tethered with NPs through covalent or coordinative interactions. Conformational entropic and enthalpic interactions are generated after grafting the polymer onto the NPs.[43–46] The energetic contributions can be adjusted by controlling the average molecular weight (M_n), architecture, chemical properties, and the surrounding solvent of the polymer. Thus, the adjacent spacing of the NPs is significantly expanded by modifying the polymer. In the last few decades, a great deal of effort has been dedicated to studying the self-organization of polymer-tethered NPs into well-defined superlattices. For example, Zhu and co-workers prepared three different types of BNSLs by controlling the M_n of polymer ligands and explained the features of two kinds of polymer-tethered spherical NPs during assembly and the corresponding co-assembly mechanism.[47]

In the past, we reported exquisite BNSLs assembled from polymer-tethered anisotropic and isotropic NPs and systematic research on the co-assembly of the different NPs and the corresponding physical mechanism.[35,37] Herein, we study the assembly of two kinds of polystyrene (PS) tethered isotropic spherical gold nanoparticles (AuNPs@PS) through the emulsion-confined assembly strategy and explore the effect of the number ratio and size ratio of the two NPs on the final internal structure of the BNSLs, which are different from our previous report.[35,37] The large AuNPs@PS building blocks are arrayed in a hexagonally close-packed or square structure, while smaller AuNP building blocks occupy the center of the periodically
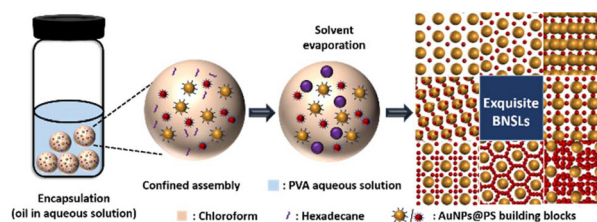
arranged large AuNP structure. Through the control of the effective size ratios and the number ratios of the two types of AuNPs, BNSLs with different internal periodic arrangements can be fabricated. Moreover, the BNSLs with diverse packing densities can be realized by tuning the M_n of the PS ligands modified on the surface of the AuNPs. After introducing long PS ligands, binary NPs are separated into macrophase separation or mixed together, depending on the interaction between polymer chains tethered to AuNPs, and the interparticle space between large AuNPs is tunable. Studying BNSLs assembled from polymer-tethered NPs may create new collective properties and provide more potential applications in data storage and optoelectronic devices.

Results and discussion

Effect of number ratios on the BNSLs

First, monodisperse AuNPs with two sizes (the average sizes are 15.4 ± 0.9 nm and 5.1 ± 0.4 nm, respectively) are synthesized according to previous literature (Fig. 1a and Fig. S1 in the ESI†),[48] and thiol-terminated PS_{2k} (PS_{2k}-SH, M_n = 2.0 kg mol^{-1}, and PDI = 1.35) are modified on the surface of the AuNPs to fabricate PS_{2k} coated $Au_{15.4}$NP ($Au_{15.4}$NPs@PS_{2k}) and PS_{2k} coated $Au_{5.1}$NP ($Au_{5.1}$NPs@PS_{2k}) building blocks (the subscripts refer to the diameter of the synthesized AuNPs) by the ligand exchange strategy.[48] Well-defined BNSLs can be prepared, as shown in Scheme 1. Typically, $Au_{15.4}$NPs@PS_{2k} building blocks, $Au_{5.1}$NPs@PS_{2k} building blocks, and hexadecane in chloroform (CF) solution (1.0 wt%) were completely mixed in appropriate proportions. Subsequently, the NP and HD chloroform mixture was emulsified using a poly(vinyl alcohol) (PVA, 0.3 wt%, 1.0 mL) aqueous solution. As the CF slowly evaporated, the AuNPs@PS building blocks spontaneously trans-

Scheme 1 Schematic diagram of the preparation of BNSLs *via* the confined co-assembly of the PS-tethered NPs of two sizes within emulsion droplets by tuning the effective size ratios and the number ratios of the two kinds of AuNPs.

ferred to the PVA/HD interface.[35,37] The spontaneous co-assembly of two kinds of AuNPs@PS building blocks occurred upon further CF evaporation. After the CF solvent had evaporated entirely, well-defined superlattices were obtained. As shown in Fig. 1a, two high monodisperse $Au_{15.4}$NPs@PS_{2k} and $Au_{5.1}$NPs@PS_{2k} are used as building blocks to prepare AuNP superlattices, where AuNPs are arranged in a hexagonally close-packed configuration, to minimize the whole system energy. When small AuNPs@PS_{2k} and large AuNPs@PS_{2k} building blocks are mixed with a number ratio of ~1 : 1, an AB-type superlattice structure is prepared,[26] which differs from the single-component system. Low and magnified transmission electron microscopy (TEM) images (Fig. 1b and c and Fig. S2†) also show that the formed BNSLs with larger AuNP building blocks were arranged in a square sublattice and the smaller ones were positioned in the interstices. In addition, the exquisite BNSLs with a special internal structure can be proved by scanning transmission electron microscopy (STEM) and the corresponding energy-dispersive X-ray spectra (EDX) elemental mapping of Au (Fig. 1d and e), and the dark background is filled almost entirely with PS ligands. Those features demonstrate the prepared BNSLs of two kinds of AuNPs@PS_{2k} with an AB-type arrangement from the top view (Fig. 1f).

To explore the fabrication of other assemblies using identical types of NPs, we systematically changed the number ratios of the $Au_{5.1}$NPs@PS_{2k} and $Au_{15.4}$NPs@PS_{2k} building blocks, as shown in Fig. 2. When the $Au_{5.1}$NPs@PS_{2k} and $Au_{15.4}$NPs@PS_{2k} building blocks are mixed with a number ratio ~2 : 1, free-standing AB_2-type BNSLs are obtained (Fig. S3†).[45] As shown in Fig. 2a and b, the larger $Au_{15.4}$NPs@PS building blocks show a hexagonally packed arrangement, and the small $Au_{5.1}$NPs@PS are located in the interstices of three neighboring larger AuNP building blocks. The inset in Fig. 2b shows the corresponding schematic diagram of the BNSLs, illustrating regular internal permutation of AuNPs, in which individual larger AuNPs have six small AuNP neighbors. The unique BNSL structure is further confirmed by STEM characterization and the corresponding EDX elemental mapping of Au (Fig. 2c and d).

Further increasing the number ratio of $Au_{5.1}$NPs@PS_{2k} to $Au_{15.4}$NPs@PS_{2k} ~3 : 1, AB_2 (Fig. 3a and Fig. S4a†)[27] and AB_3-type BNSLs (Fig. 3b and Fig. S4b†)[26] can be prepared. Notably,
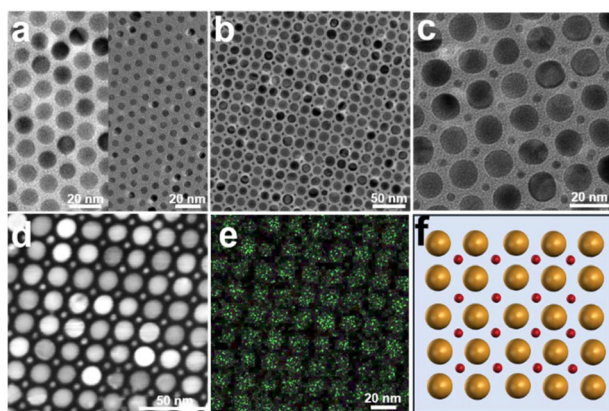

Fig. 1 (a) TEM images of the single-component superlattices assembled from $Au_{15.4}$NPs@PS_{2k} (left) and $Au_{5.1}$NPs@PS_{2k} building blocks (right), respectively. (b) Low and (c) high magnification TEM images of the BNSLs assembled from $Au_{5.1}$NPs@PS_{2k} and $Au_{15.4}$NPs@PS_{2k} building blocks at a number ratio of 1 : 1, respectively. (d) and (e) Corresponding STEM image and EDX elemental mapping of Au of the formed BNSLs, respectively. (f) Schematic illustration of the periodic internal permutation of the BNSLs.
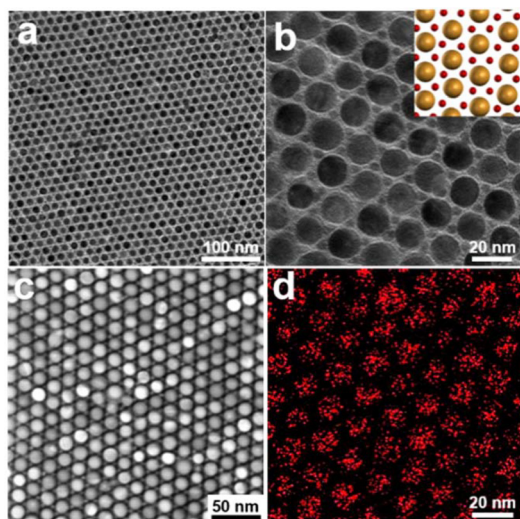
Fig. 2 (a) Low and (b) high magnification TEM images of the BNSLs assembled from $Au_{5.1}NPs@PS_{2k}$ and $Au_{15.4}NPs@PS_{2k}$ building blocks at a number ratio of 2 : 1. The inset in (b) shows the corresponding schematic diagram of the internal arrangement of AuNPs within BNSLs. (c) and (d) Corresponding STEM image and EDX elemental mapping of Au of the BNSLs, respectively.
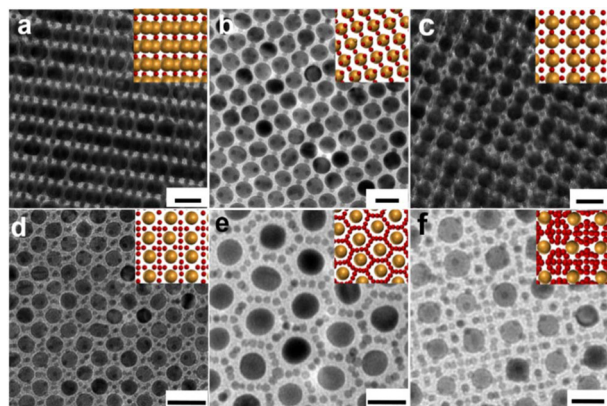

Fig. 3 (a–f) TEM images of BNSLs from different mixing ratios of small AuNPs (5.1 nm in diameter) and large AuNPs (15.4 nm in diameter) with the following phases: (a) AB_2-type, 3 : 1; (b) AB_3-type, 3 : 1; (c) Cu_3Au-type, 7 : 1; (d) CaB_6-type, 7 : 1; (e) small AuNPs around the larger AuNPs, 7 : 1; and (f) $NaZn_{13}$-type, 13 : 1. The inset images show the schematic diagram according to the corresponding BNSLs and the scale bars are 20 nm.

when the number ratio of the mixture increases to ~7 : 1, Cu_3Au-type (Fig. 3c),[42] CaB_6-type (Fig. 3d),[36] and the structure of small AuNPs around the larger AuNPs (Fig. 3e and Fig. S4c†) can be obtained. Further increasing the number ratio of the small AuNPs and large AuNPs to ~13 : 1 results in phase-pure BNSLs of higher stoichiometries, *i.e.*, $NaZn_{13}$,[42] which exhibits the cubic symmetry and the long-range arrangement of the two types of AuNPs (Fig. 3f and Fig. S4d†). It is worth noting that although these BNSLs have been prepared by previous methods,[26,42] achieving eight kinds of BNSLs with

different internal structures using NPs with a single effective size ratio is still a challenge.

As previously reported,[35,37] the formation of well-defined BNSLs is determined by minimizing the Gibbs free energy. The overall change in the Gibbs free energy of the AuNPs@PS system can be expressed as:

$$\Delta G = \Delta H - T\Delta S \qquad (1)$$

where ΔH refers to the enthalpic energy change, which is mainly determined by the interaction among the building blocks, and T is the temperature in Kelvin. ΔS is the entropic energy change, which mainly depends on the conformation entropy of the polymer chains (ΔS_{con}) and the mixing entropy of the NPs of two sizes (ΔS_{mix}). For the NPs with 5.1 nm, they can easily move into the lattice formed by the NPs with 15.4 nm. In this case, the contribution of ΔS_{con} can be ignored, and ΔS_{mix} plays a key role in forming the BNSLs. It drives the smaller AuNPs into the lattice formed by bigger AuNPs. Moreover, the distribution of smaller AuNPs in the lattice is as uniform as possible to maximize ΔS_{mix}, thereby minimizing the free energy. When the number ratio is 1 : 1, an AB-type superlattice structure is prepared, as shown in Fig. 1. AB-type BNSLs have the most uniform distribution to minimize the Gibbs free energy. Similarly, the lattices in the small NPs are uniformly distributed around the big NPs, *i.e.*, AB_2-type, AB_3-type, Cu_3Au-type, and CaB_6-type can be obtained by increasing the number ratio up to 7 : 1. However, if the ratio is increased to 13 : 1, the small NPs are too many to be uniformly distributed around the big NPs, and the excess small NPs have to aggregate into the vertices formed by four big NPs uniformly. Therefore, an $NaZn_{13}$-type superlattice can be obtained, as shown in Fig. 3f.

Effect of size ratios on the BNSLs

In addition to the number ratio of the two kinds of AuNPs@PS building blocks, the effective size ratio of AuNPs@PS (λ_{eff}), the ratio of the effective diameter of the PS tethered small AuNPs (d_{eff}) to that of the PS tethered large AuNPs (D_{eff}), also plays a dominant role in the configuration of the BNSLs. λ_{eff} can be applied to access the loss of entropy after the introduction of the small AuNPs. The effective diameter of the AuNPs@PS building blocks including the NP core and PS shell can be measured as the center-point to center-point distance between the adjacent AuNPs@PS building blocks from single-component AuNP@PS hexagonal packing in TEM images (Fig. S5d†). Herein, AuNPs with various diameters (*i.e.*, 1.7 nm, 8 nm, and 10 nm) were prepared (Fig. S5a–c†) and tethered with PS_{2k}, and further co-assembly with $Au_{15.4}NPs@PS_{2k}$ with a fixed number ratio of 2 : 1 to explore the effect of λ_{eff} on the structure of the BNSLs.[48,49] For the $Au_{1.7}NPs@PS_{2k}$ (d_{eff} = 4.1 ± 0.6 nm) and $Au_{15.4}NPs@PS_{2k}$ (D_{eff} = 20.1 ± 1.3 nm) building blocks, λ_{eff} is thus calculated to be 0.2, and $Au_{1.7}NPs@PS_{2k}$ building blocks are distributed in the gap between the $Au_{15.4}NPs@PS_{2k}$ building blocks (Fig. 4a). In this case, as the diameter of $Au_{1.7}NPs@PS_{2k}$ is so small, the conformational

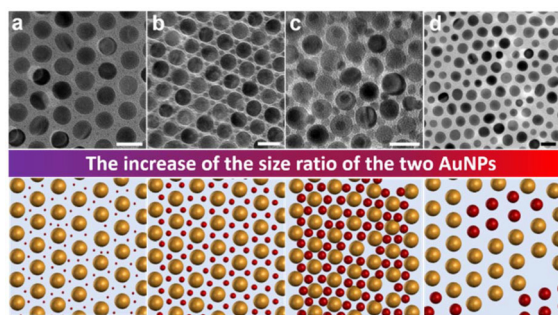**Fig. 4** TEM images (top images) and the corresponding schematic diagrams (bottom images) displaying BNSLs assembled from the $Au_{15.4}NPs@PS_{2k}$ building blocks and $AuNPs@PS_{2k}$ with different core diameters, keeping the other conditions unchanged ($Au_{15.4}NPs@PS_{2k} : AuNPs@PS_{2k} = 1:2$). (a) $Au_{1.7}NPs@PS_{2k}$; (b) $Au_{5.1}NPs@PS_{2k}$; (c) $Au_8NPs@PS_{2k}$; and (d) $Au_{10}NPs@PS_{2k}$. The scale bars are 20 nm.

Fig. 5 (a–c) TEM images showing BNSLs assembled from $Au_{15.4}NPs@PS_{2k}$ and $Au_{5.1}NPs@PS$ building blocks tethered with PS ligands of different M_n, keeping the other conditions unchanged ($Au_{15.4}NPs@PS_{2k} : Au_{5.1}NPs@PS = 1:2$). (a) PS_{2k}; (b) PS_{5k}; and (c) PS_{12k}. The scale bars are 20 nm.

entropy of the introduced $Au_{1.7}NPs@PS_{2k}$ can be ignored. Thus, the $Au_{15.4}NPs@PS_{2k}$ building blocks maintain the hexagonal packing to minimize the whole Gibbs free energy of the BNSLs. After the increase of the core AuNP size to 5.1 nm (*i.e.*, $Au_{5.1}NPs@PS_{2k}$, $d_{eff} = 8.7 \pm 0.8$ nm), the calculated λ_{eff} is 0.4, and the BNSLs exhibit the aforementioned AB_2-type arrangement (Fig. 2 and 4b). After d_{eff} further increases to 11.2 ± 0.8 nm (*i.e.*, $Au_8NPs@PS_{2k}$), λ_{eff} is 0.5 and exquisite BNSLs can be prepared, as shown in Fig. 4c. In this case, $Au_{15.4}NPs@PS_{2k}$ still shows a hexagonally packed arrangement, and $Au_8NPs@PS_{2k}$ is positioned in the space surrounded by three neighboring $Au_{15.4}NPs@PS_{2k}$ building blocks, whereas the packing density increases compared with λ_{eff} which is 0.4. However, if oversized $AuNPs@PS_{2k}$ (*i.e.*, $Au_{10}NPs@PS_{2k}$, $d_{eff} = 13.5 \pm 0.5$ nm, and λ_{eff} is 0.7) is used, the introduced $Au_{10}NPs@PS_{2k}$ causes the loss of conformational entropy, so $Au_{10}NPs@PS_{2k}$ is macroscopically separated from the hexagonal $Au_{15.4}NPs@PS_{2k}$ matrix to reduce the global free energy (Fig. 4d). In particular, when the number ratio of $Au_{10}NPs@PS_{2k}$ to $Au_{15}NPs@PS_{2k}$ increases to ~10:1, $CaCu_5$-type BNSLs can be obtained,[26] as shown in Fig. S6.† The results show that both the number ratio and effective size ratio of the NPs have a decisive effect on the final internal structure of BNSLs.

In addition to the diameter of the initial synthesized NPs, the thickness of PS ligands also contributes to the d_{eff} of $AuNPs@PS$ as well as λ_{eff}, affecting the arrangement of NPs within the assemblies. Therefore, $Au_{5.1}NPs$ tethered with different PS ligands are synthesized (*i.e.*, PS_{2k}, PS_{5k}, and PS_{12k}) to investigate the impact of the thickness of the PS ligands modified on the surface of $Au_{5.1}NPs$ building blocks on the final distribution of the BNSLs (Fig. S7†). Based on the previous discussion, $Au_{15.4}NPs@PS_{2k}$ and $Au_{5.1}NPs@PS_{2k}$ are assembled into an AB_2-type structure (Fig. 5a). With a further increase of M_n of the PS ligands to 5k (*i.e.*, $Au_{5.1}NPs@PS_{5k}$), the d_{eff} value increases to 13.3 ± 0.9 nm, and the calculated λ_{eff} is 0.7. $Au_{15.4}NPs@PS_{2k}$ still shows a hexagonal configuration and $Au_{5.1}NPs@PS_{5k}$ is mainly irregularly distributed in the ver-
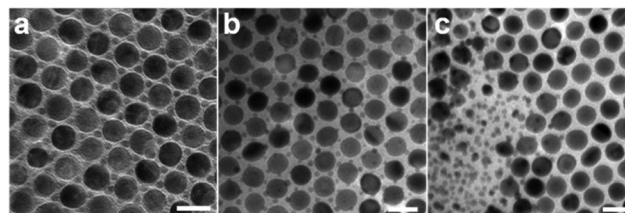
tices formed by three adjacent $Au_{15.4}NPs@PS_{2k}$ building blocks (Fig. 5b), which is different from the result in Fig. 4d, attributed to the partially or fully screened rigid nature of small NPs. With a further increase in the M_n of PS ligands to 12k, the d_{eff} is 17.2 ± 1.7 nm, and the λ_{eff} is 0.9. In this case, the $Au_{15.4}NPs@PS_{2k}$ and $Au_{5.1}NPs@PS_{12k}$ building blocks form a disordered state, as shown in Fig. 5c. At this time, the narrow space between $Au_{15.4}NPs@PS_{2k}$ cannot be penetrated by $Au_{5.1}NPs@PS_{12k}$. On the other hand, the short polymer-tethered large AuNPs quickly settle *via* the evaporation of the CF, while the long polymer-tethered small AuNPs are still well dispersed.

Similarly, large $Au_{15.4}NPs$ tethered with PS ligands of different M_n (*i.e.*, $PS_{0.8k}$, PS_{5k}, and PS_{12k}) and $Au_{5.1}NPs@PS_{2k}$ are synthesized (Fig. S8†) and co-assembled with a number ratio of 1:2 to further explore their final spatial distribution of the BNSLs. When $Au_{15.4}NPs@PS_{0.8k}$ ($D_{eff} = 19.6 \pm 1.2$ nm and $\lambda_{eff} = 0.4$) are used to co-assemble with $Au_{5.1}NPs@PS_{2k}$, macroscopic phase separation is caused and almost no regular BNSLs can be noted, which is probably because $Au_{5.1}NPs@PS_{2k}$ cannot penetrate the short $PS_{0.8k}$ brushes on the surface of large AuNPs (Fig. 6a). As PS ligands increase to
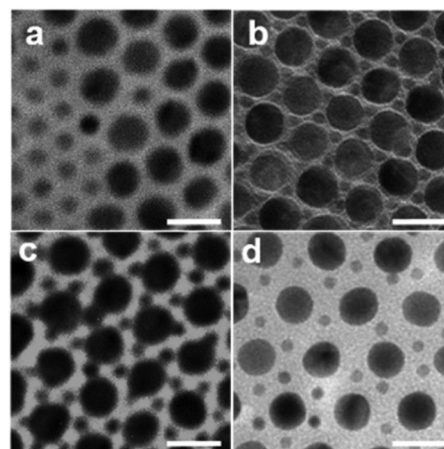

Fig. 6 (a–d) TEM images exhibiting the assemblies formed from $Au_{5.1}NPs@PS_{2k}$ and $Au_{15.4}NPs$ tethered with PS ligands of different M_n, keeping the other conditions unchanged ($Au_{15.4}NPs@PS : Au_{5.1}NPs@PS_{2k} = 1:2$). (a) $PS_{0.8k}$; (b) PS_{2k}; (c) PS_{5k}; and (d) PS_{12k}. The scale bars are 20 nm.

5k (Au$_{15.4}$NPs@PS$_{5k}$, D_{eff} = 21.5 ± 1.4 nm, and λ_{eff} = 0.4), at this time, AB$_2$-type BNSLs can be prepared (Fig. 6c). With a further increase in the M_n of PS ligands to 12k (Au$_{15.4}$NPs@PS$_{12k}$, D_{eff} = 26.2 ± 0.9 nm, and λ_{eff} = 0.3), the formed BNSLs adopt an AB$_2$-type structure (Fig. 6d). However, the small AuNPs within the BNSLs are not evenly distributed in the space surrounded by three adjacent large AuNPs because the increase of M_n of PS ligands provides more space to accommodate small AuNPs and the AB$_2$-type structure is not close-packed. Through tuning of the M_n of the large AuNPs, AB$_2$-type BNSLs with different stacking densities of AuNPs of two sizes can be prepared. For further exploring the size ratio and number ratio of the two kinds of AuNPs@PS building blocks, Au$_{15.4}$NPs@PS$_{0.8k}$ and Au$_{15.4}$NPs@PS$_{12k}$ are co-assembled with more Au$_{5.1}$NPs@PS$_{2k}$, and the results in Fig. S9† show that exquisite BNSLs can be fabricated through tuning the size ratio and number ratio of the two kinds of AuNPs. As shown in Fig. S9a,† when Au$_{15.4}$NPs@PS$_{0.8k}$ building blocks are co-assembled with Au$_{5.1}$NPs@PS$_{2k}$ with a number ratio of ~1 : 13, AB$_{13}$-type BNSLs can be prepared. Similarly, when the number ratio of Au$_{5.1}$NPs@PS$_{2k}$ building blocks and Au$_{15.4}$NPs@PS$_{12k}$ increases, the structure of small NPs around Au$_{15.4}$NPs@PS$_{12k}$ is prepared (Fig. S9b†). The study shows that the internal structure should be predicted using size and number ratios, which cannot be simply determined by one parameter.

The above results show that λ_{eff} can be applied to assess the entropy loss after introducing the small AuNPs and predict the structure of the formed BNSLs. Moreover, λ_{eff} can be adjusted through the core diameter of the AuNPs and the M_n of the PS ligands modified on the surface of the AuNPs, and the corresponding stacking density of the BNSLs can also be tuned. However, when exploring the effect of λ_{eff} on the BNSLs, the ratio of AuNPs of two sizes should be fixed. The final structure of the BNSLs is determined by the number and size ratios of the AuNPs of two sizes (Table S1†).

Conclusions

In brief, we developed a strategy to fabricate exquisite BNSLs assembled from PS-tethered spherical AuNPs in two sizes. The large AuNPs display a square or hexagonal stacking arrangement in BNSLs, while the introduced small AuNPs@PS are located in the PS domain surrounded by adjacent large ones to minimize the total free energy. In this strategy, the final distributions of the two diameters of AuNPs within the BNSLs mainly depend on the number ratios and the effective size ratio of the AuNPs. By adjusting the number ratio of the two diameters of AuNPs, eight kinds of BNSLs with different internal structures can be prepared. However, when the number ratio remains at 2 : 1, by tuning the effective size ratio, the obtained AlB$_2$-type BNSLs remain unchanged until the effective size ratio reaches 0.5. In particular, when the number ratio of the two AuNPs changes (Au$_{15.4}$NPs@PS$_{2k}$: Au$_{5.1}$NPs@PS$_{2k}$ ~1 : 13), the phase separation structure becomes an ordered structure. Our results show that both the number ratio and effective size ratio of

the AuNPs dominate the ultimate structures of the BNSLs, providing helpful guidance for the design of BNSLs.

Data availability

The data supporting this article have been included as part of the ESI.†

Conflicts of interest

The authors declare no conflicts of interest.

Acknowledgements

References

1 S. Mourdikoudis, M. Menelaou, N. Fiuza-Maneiro, G. C. Zheng, S. Y. Wei, J. Pérez-Juste, L. Polavarapu and Z. Sofer, *Nanoscale Horiz.*, 2022, **7**, 941–1015.

2 Y. Wang, J. Chen, C. Zhu, B. Zhu, S. Jeong, Y. Yi, Y. Liu, J. Fiadorwu, P. He and X. Ye, *Nano Lett.*, 2021, **21**, 5053–5059.

3 K. Wang, H. Ling, Y. Bao, M. Yang, Y. Yang, M. Hussain, H. Wang, L. Zhang, L. Xie, M. Yi, W. Huang, X. Xie and J. Zhu, *Adv. Mater.*, 2018, **30**, e1800595.

4 Q. Shi, D. Sikdar, R. Fu, K. J. Si, D. Dong, Y. Liu, M. Premaratne and W. Cheng, *Adv. Mater.*, 2018, **30**, e1801118.

5 F. Schulz, O. Pavelka, F. Lehmkuhler, F. Westermeier, Y. Okamura, N. S. Mueller, S. Reich and H. Lange, *Nat. Commun.*, 2020, **11**, 3821.

6 Z. Nie, A. Petukhova and E. Kumacheva, *Nat. Nanotechnol.*, 2010, **5**, 15–25.

7 M. Marchioni, G. Veronesi, I. Worms, W. L. Ling, T. Gallon, D. Leonard, C. Gateau, M. Chevallet, P. H. Jouneau, L. Carlini, C. Battocchio, P. Delangle, I. Michaud-Soret and A. Deniaud, *Nanoscale Horiz.*, 2020, **5**, 507–513.

8 K. H. Ku, J. M. Shin, M. P. Kim, C. H. Lee, M. K. Seo, G. R. Yi, S. G. Jang and B. J. Kim, *J. Am. Chem. Soc.*, 2014, **136**, 9982–9989.

9 Y. Kang, X. Ye, J. Chen, Y. Cai, R. E. Diaz, R. R. Adzic, E. A. Stach and C. B. Murray, *J. Am. Chem. Soc.*, 2013, **135**, 42–45.

10 S. Gupta, Q. Zhang, T. Emrick, A. C. Balazs and T. P. Russell, *Nat. Mater.*, 2006, **5**, 229–233.

11 A. Dong, J. Chen, P. M. Vora, J. M. Kikkawa and C. B. Murray, *Nature*, 2010, **466**, 474–477.

12 I. Cherniukh, G. Raino, T. V. Sekh, C. Zhu, Y. Shynkarenko, R. A. John, E. Kobiyama, R. F. Mahrt, T. Stoferle, R. Erni,

M. V. Kovalenko and M. I. Bodnarchuk, *ACS Nano*, 2021, **15**, 16488–16500.

13 S. Brittman, N. A. Mahadik, S. B. Qadri, P. Y. Yee, J. G. Tischler and J. E. Boercker, *ACS Appl. Mater. Interfaces*, 2020, **12**, 24271–24280.

14 H. Yun, J. W. Yu, Y. J. Lee, J.-S. Kim, C. H. Park, C. Nam, J. Han, T.-Y. Heo, S.-H. Choi, D. C. Lee, W. B. Lee, G. E. Stein and B. J. Kim, *Chem. Mater.*, 2019, **31**, 5264–5273.

15 M. Xu, K. H. Ku, Y. J. Lee, T. Kim, J. J. Shin, E. J. Kim, S.-H. Choi, H. Yun and B. J. Kim, *Macromolecules*, 2021, **54**, 3084–3092.

16 H. Wang, H. Qian, W. Li, K. Wang, H. Li, X. Zheng, P. Gu, S. Chen, M. Yi, J. Xu and J. Zhu, *Small*, 2023, **19**, e2208288.

17 K. Thorkelsson, J. H. Nelson, A. P. Alivisatos and T. Xu, *Nano Lett.*, 2013, **13**, 4908–4913.

18 C. Wang, *Nanoscale Horiz.*, 2024, **9**, 1853–1854.

19 Z. Nie, D. Fava, E. Kumacheva, S. Zou, G. C. Walker and M. Rubinstein, *Nat. Mater.*, 2007, **6**, 609–614.

20 R. Liang, J. Xu, R. Deng, K. Wang, S. Liu, J. Li and J. Zhu, *ACS Macro Lett.*, 2014, **3**, 486–490.

21 F. Li, K. Wang, N. Deng, J. Xu, M. Yi, B. Xiong and J. Zhu, *ACS Appl. Mater. Interfaces*, 2021, **13**, 6566–6574.

22 J. Kao and T. Xu, *J. Am. Chem. Soc.*, 2015, **137**, 6356–6365.

23 J. Gong, R. S. Newman, M. Engel, M. Zhao, F. Bian, S. C. Glotzer and Z. Tang, *Nat. Commun.*, 2017, **8**, 14038.

24 Y. Gao, Y. Zhou, X. Xu, C. Chen, B. Xiong and J. Zhu, *Small*, 2022, e2106880, DOI: 10.1002/smll.202106880.

25 C. Yi, Y. Yang, B. Liu, J. He and Z. Nie, *Chem. Soc. Rev.*, 2020, **49**, 465–508.

26 X. Ye, C. Zhu, P. Ercius, S. N. Raja, B. He, M. R. Jones, M. R. Hauwiller, Y. Liu, T. Xu and A. P. Alivisatos, *Nat. Commun.*, 2015, **6**, 10052.

27 E. V. Shevchenko, D. V. Talapin, N. A. Kotov, S. O'Brien and C. B. Murray, *Nature*, 2006, **439**, 55–59.

28 Y. Chen, T. W. Liang, L. Chen, Y. F. Chen, B. R. Yang, Y. H. Luo and G. S. Liu, *Nanoscale Horiz.*, 2022, **7**, 1299–1339.

29 X. Lin, S. Ye, C. Kong, K. Webb, C. Yi, S. Zhang, Q. Zhang, J. T. Fourkas and Z. Nie, *J. Am. Chem. Soc.*, 2020, **142**, 17282–17286.

30 W. Li, K. Wang, P. Zhang, J. He, S. Xu, Y. Liao, J. Zhu, X. Xie and Z. Nie, *Small*, 2016, **12**, 499–505.

31 J. Kao, P. Bai, J. M. Lucas, A. P. Alivisatos and T. Xu, *J. Am. Chem. Soc.*, 2013, **135**, 1680–1683.

32 C. Jenewein, J. Avaro, C. Appel, M. Liebi and H. Colfen, *Angew. Chem., Int. Ed.*, 2022, **61**, e202112461.

33 W. Dong, Y. Zhang, C. Yi, J. J. Chang, S. Ye and Z. Nie, *ACS Nano*, 2023, **17**, 3047–3054.

34 P. Bai, S. Yang, W. Bao, J. Kao, K. Thorkelsson, M. Salmeron, X. Zhang and T. Xu, *Nano Lett.*, 2017, **17**, 6847–6854.

35 X. Yue, J. Li, N. Yan and W. Jiang, *Small*, 2023, **19**, 2207984.

36 F. Rechberger and M. Niederberger, *Nanoscale Horiz.*, 2017, **2**, 6–30.

37 J. Li, X. Yu, J. Zhang, N. Yan, J. Jin and W. Jiang, *ChemComm*, 2023, **59**, 12338–12341.

38 J. Li, X. Liu, J. Jin, N. Yan and W. Jiang, *Nanotechnology*, 2022, **33**, 385601.

39 X. Dai, H.-X. Wan, X. Zhang, W. Wei, W. Chen, L. Zhang, J. Li and L.-T. Yan, *Chem. Res. Chin. Univ.*, 2023, 709–718.

40 M. I. Bodnarchuk, E. V. Shevchenko and D. V. Talapin, *J. Am. Chem. Soc.*, 2011, **133**, 20837–20849.

41 C. Yi, H. Liu, S. Zhang, Y. Yang, Y. Zhang, Z. Lu, E. Kumacheva and Z. Nie, *Science*, 2020, **369**, 1369–1374.

42 X. Ye, J. Chen, B. T. Diroll and C. B. Murray, *Nano Lett.*, 2013, **13**, 1291–1297.

43 X. Zhang, X. Dai, L. Gao, D. Xu, H. Wan, Y. Wang and L.-T. Yan, *Chem. Soc. Rev.*, 2023, **52**, 6806–6837.

44 C. Yi, Y. Yang and Z. Nie, *J. Am. Chem. Soc.*, 2019, **141**, 7917–7925.

45 A. Dong, X. Ye, J. Chen and C. B. Murray, *Nano Lett.*, 2011, **11**, 1804–1809.

46 M. I. Bodnarchuk, M. V. Kovalenko, W. Heiss and D. V. Talapin, *J. Am. Chem. Soc.*, 2010, **132**, 11967–11977.

47 K. Wang, F. Li, S.-M. Jin, K. Wang, D. Tian, M. Hussain, J. Xu, L. Zhang, Y. Liao, E. Lee, G.-R. Yi, X. Xie and J. Zhu, *Mater. Chem. Front.*, 2020, **4**, 2089–2095.

48 Y. Zheng, X. Zhong, Z. Li and Y. Xia, *Part. Part. Syst. Charact.*, 2014, **31**, 266–273.

49 M. Brust, M. Walker, D. Bethell, D. J. Schiffrin and R. Whyman, *J. Chem. Soc., Chem. Commun.*, 1994, 801–802.